Cancer Cell
Article

# Modeling Inducible Human Tissue Neoplasia Identifies an Extracellular Matrix Interaction Network Involved in Cancer Progression

Jason A. Reuter,[1,2,3] Susana Ortiz-Urda,[1,3] Markus Kretz,[1,3] John Garcia,[1,3,4] Florence A. Scholl,[1,3] Anna M.G. Pasmooij,[1,3] David Cassarino,[5] Howard Y. Chang,[3,4] and Paul A. Khavari[1,3,4,*]
[1]Veterans Affairs Palo Alto Healthcare System, Palo Alto, CA 94306, USA
[2]Department of Genetics
[3]Program in Epithelial Biology
[4]Program in Cancer Biology
Stanford University School of Medicine, Stanford, CA 94305, USA
[5]Department of Pathology and Laboratory Medicine, University of California, Los Angeles, Los Angeles, CA 90095, USA
*Correspondence: khavari@stanford.edu
DOI 10.1016/j.ccr.2009.04.002

## SUMMARY

**To elucidate mechanisms of cancer progression, we generated inducible human neoplasia in three-dimensionally intact epithelial tissue. Gene expression profiling of both epithelia and stroma at specific time points during tumor progression revealed sequential enrichment of genes mediating discrete biologic functions in each tissue compartment. A core cancer progression signature was distilled using the increased signaling specificity of downstream oncogene effectors and subjected to network modeling. Network topology predicted that tumor development depends on specific extracellular matrix-interacting network hubs. Blockade of one such hub, the β1 integrin subunit, disrupted network gene expression and attenuated tumorigenesis in vivo. Thus, integrating network modeling and temporal gene expression analysis of inducible human neoplasia provides an approach to prioritize and characterize genes functioning in cancer progression.**

## INTRODUCTION

Progression from normal, basement membrane (BM)-bound epithelium to invasive cancer characterizes most human neoplasms, including lung, breast, prostate, colon, kidney, bladder, and skin, and is a central requirement for biologic malignancy. This process involves tumor-stroma coevolution in which both epithelial cells and their stromal microenvironment undergo a sequential series of morphologic changes (Littlepage et al., 2005). In epithelium, these changes commonly involve premalignant hyperplasia, followed by in situ neoplasia confined above the epithelial BM, and then invasion of neoplastic epithelial cells across the BM into surrounding stroma (Alam and Ratner, 2001). Stromal changes include an influx of inflammatory cells, alterations in extracellular matrix (ECM) architecture, and increased angiogenesis, cancer-enabling processes that stromal cells help facilitate (Mueller and Fusenig, 2004; Orimo et al., 2005). Further characterizing the interactions between these two tissue compartments may help arrest epithelial tumor progression early in its course.

Epidermal skin cancers serve as prototypes of epithelial tumor-stroma progression and are nearly as common as all other U.S. cancers combined (Lewis and Weinstock, 2007). Human tissue models for squamous cell carcinoma (SCC) have been produced by combining normal human dermal stroma with primary human epidermal keratinocytes engineered to express

### SIGNIFICANCE

Investigating tumor progression in patient samples is complicated by etiologic heterogeneity, genetic instability, and an overabundance of precursor lesions that fail to progress. These complexities obscure construction of a dynamic picture of progression from normal tissue to invasive cancer. Here, inducible human neoplasia driven by conditionally active Ras is generated, and the sequence of gene expression programs engaged in epithelial tumor tissue and adjacent stroma during carcinogenesis is characterized. Tumor-intrinsic gene expression can be refined by sufficient downstream oncogene effectors and a generalizable network modeling strategy can be applied to prioritize targets based on local interconnectivity. This analysis highlights the importance of tumor-stroma interaction during tumorigenesis and identifies β1 integrin as a potential oncotherapeutic that distinguishes normal and neoplastic tissue.

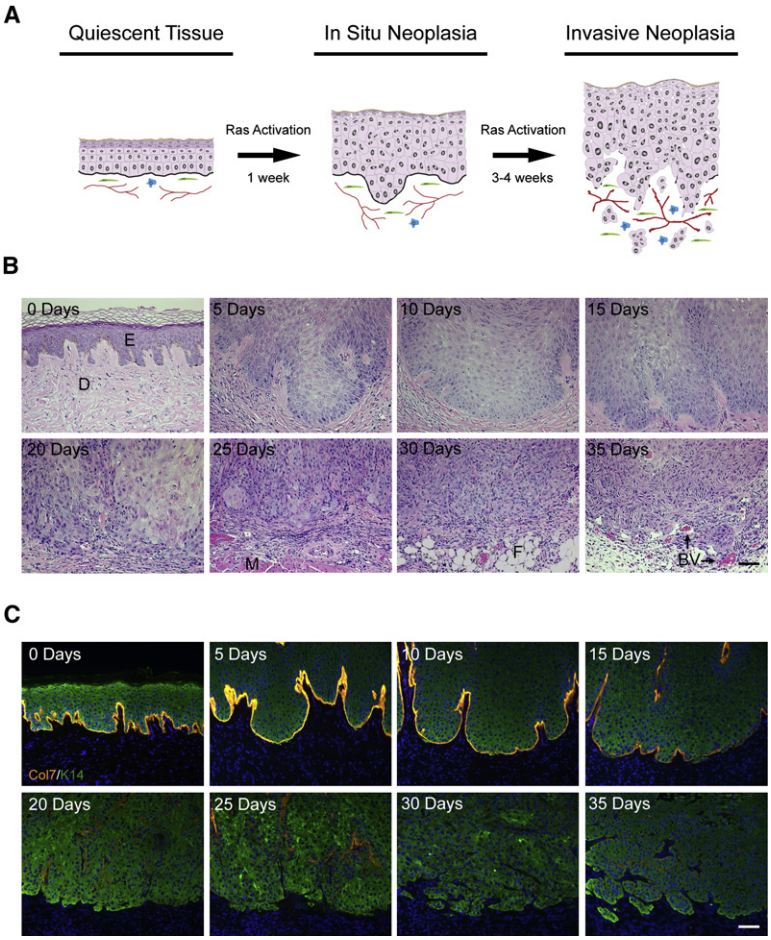


**Figure 1. Inducible Progression of Human Tissue Neoplasia**

(A) Schematic of inducible human tissue neoplasia.

(B) Histology of ER:Ras-IκBα regenerated human tissue after the indicated durations of 4OHT treatment. Note the SCC in situ-like disruption of epidermal polarity and differentiation evident by day 10 as well as the progressive invasion of epithelial cells into the underlying stroma from days 20 to 35. Scale bar, 125 μm. E, Epidermis; D, dermis; F, fat; M, muscle; BV, blood vessels.

(C) Immunostains on tissue from (B) using antibodies against the BM protein, type VII collagen (Col7; orange), and the epithelial marker, keratin 14 (K14; green). Note the progressive loss of BM integrity as the epithelial cells invade into the underlying dermis. Scale bar, 125 μm.

cancer-associated genes and grafting the resultant tissue onto an immune-deficient mouse (Khavari, 2006). Transformation in this setting was achieved by coexpressing oncogenic Ras with a mediator of G1 cell cycle escape, such as Cdk4, JNK, or IκBα. Importantly, malignancy is defined in this tissue context similarly to clinical specimens, namely invasion through an intact BM into the underlying stroma. Moreover, genomic instability has not been observed in these initial models (Wong et al., 2008), making the study of oncogenic signaling networks free of potentially confounding secondary genetic alterations.

Cancers display large differences in gene expression from normal tissue and, yet, attributing biologic significance to any one gene in isolation is difficult. It is increasingly appreciated, however, that complex networks govern cellular behavior (Albert et al., 2000) and several lines of evidence suggest that understanding the organization of such networks may help discover genes required for tumor progression. First, a number of studies demonstrate a correlation between a protein's degree, or number of interactions, and its probability of being essential (Jeong et al., 2001; Lee et al., 2008). Second, somatic cancer genes, unlike congenital human disease genes, tend to encode proteins of high degree (Jonsson and Bates, 2006). Finally, targets of FDA-approved drugs are significantly more interconnected than random network components (Yildirim et al., 2007). Systematic efforts to manually curate known biology have organized vast amounts of data describing potential interactions between genes and/or proteins (Ganter and Giroux, 2008). Integrating this information with gene expression signatures obtained at discrete steps in tumor progression may help prioritize targets for functional validation in model systems of human tumorigenesis.

## RESULTS

### Inducible Human Model of Progression to Invasive Neoplasia

To precisely investigate the temporal progression of quiescent human epithelial tissue to invasive cancer, we generated an inducible model of epidermal neoplasia (Figure 1A). To do this, a 4-hydroxytamoxifen (4OHT) responsive form of oncogenic H-Ras (ER:Ras) was coexpressed with IκBα in human epidermis regenerated on human dermal tissue and grafted to immune-deficient mice. Uninduced ER:Ras-IκBα epidermis exhibited normal tissue polarity and BM protein distribution (Figures 1B and 1C). Upon Ras activation, however, the epidermal tissue progressively underwent changes characteristic of SCC, including hyperproliferation, aberrant tissue polarity and differentiation, increased angiogenesis, and ultimately epithelial cell invasion through the BM into the underlying host dermis, fat, and muscle (Figure 1B). These changes mimicked the progression of human epidermis to SCC in situ and then to invasive SCC. Immunostains for type VII collagen confirmed BM disruption and invasion into underlying stroma (Figure 1C). The kinetics of tumor progression were rapid; hyperplasia and disordered tissue polarity consistent with SCC in situ were evident by days 5 to 10 and culminated in a fully manifest invasive phenotype by days 25 to 30. ER:Ras-IκBα invasive tumors were histologically and immunophenotypically indistinguishable from constitutive Ras-IκBα-driven SCCs (Dajee et al., 2003), suggesting that, despite tamoxifen's use as an oncotherapeutic in breast cancer, 4OHT does not significantly alter tumorigenesis in our model. Thus, conditional Ras activation in the context of G1 escape mechanisms models the progression of human epidermal tissue from quiescent to invasive neoplasia.

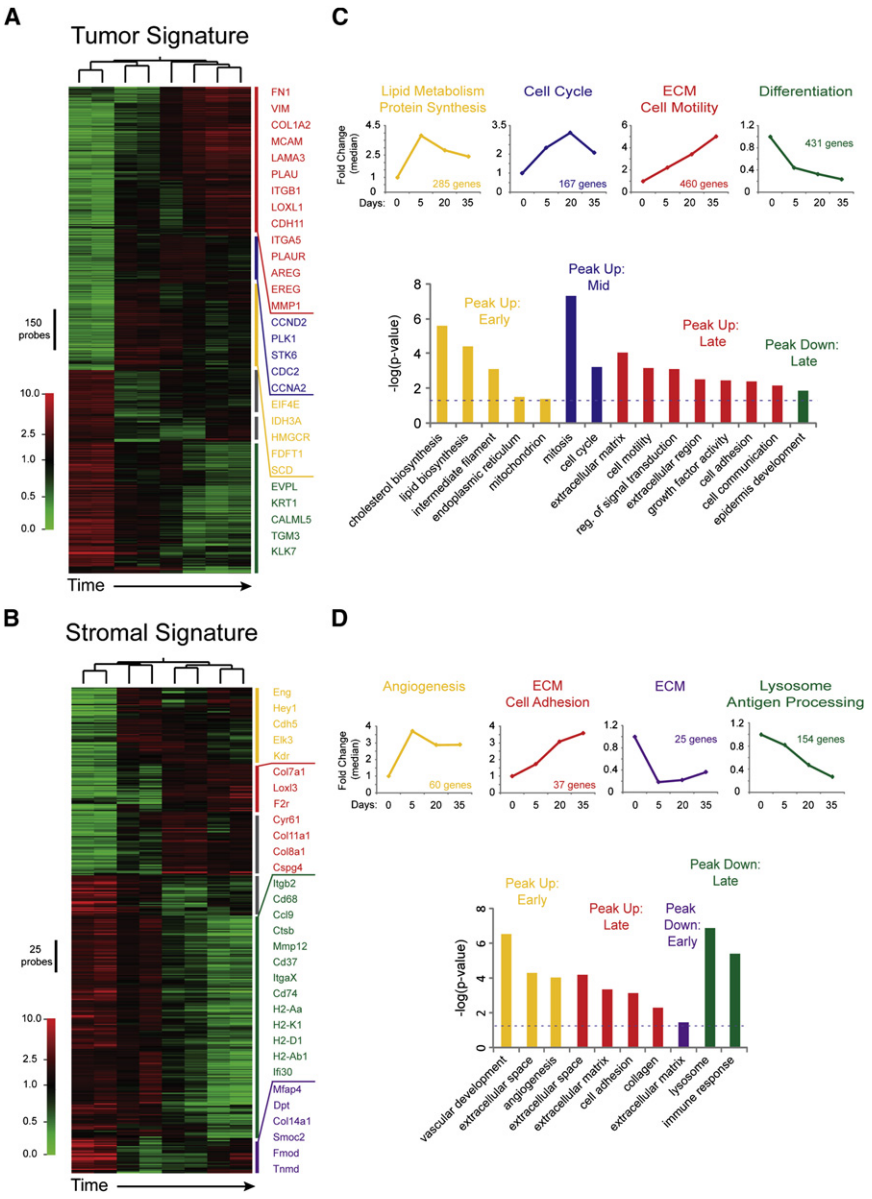


**Figure 2. Tumor and Stromal Gene Expression during Tumor Progression**

(A and B) LCM-mediated microarray analysis of epithelial and stromal RNA isolated from ER:Ras-IκBα grafts after 0, 5, 20, and 35 days of Ras induction. Each time point was done in duplicate. Differentially expressed probes were mean centered, hierarchically clustered, and colored red (induced) and green (repressed) based on a $\log_2$ scale. Clustering of the arrays based on these differentially expressed probes recapitulated the temporal order that the samples were taken during tumor progression. The dendogram at the top represents the extent of similarity among array samples. The bars to the right of the heat map demarcate boundaries between temporal expression clusters. Selected genes for each cluster are color coded and listed to the right of each heat map.

(C and D) Graphs illustrating the temporal expression profile for each epithelial or stromal gene cluster are shown (top) as a ratio of the median expression at the indicated time point relative to day 0. Significantly enriched GO terms for each cluster are represented in a histogram (bottom) as the −log ($p < 0.05$, Bonferroni-corrected EASE score). Redundant terms have been omitted for clarity. Dotted line indicates significance threshold.

## Temporal Analysis of Gene Expression in Tumor and Stroma

To characterize the gene expression changes in tumor and stroma over time, we profiled mRNA extracted from laser capture microdissected epithelial and stromal tissue after 0, 5, 20, and 35 days of Ras activation (see Figure S1A available online). Tissue dissection was restricted to the cells residing near the interface between the human epithelium and the host stroma (Figure S1B). RNA was isolated, subjected to one round of T7-based linear amplification, and hybridized to human or mouse oligonucleotide arrays. A comparison of the raw probe intensities of epithelial and stromal cell markers across both microarray data sets confirmed the two RNA populations were distinct (Figure S1C and Table S1).

Using this approach, we identified 1555 epithelial genes and 355 stromal genes differentially expressed during Ras-driven tumor progression (Figure S1D and Tables S2 and S3). Hierarchical clustering of the arrays using these gene sets reconstructed the time course of tumor progression and segregated the samples into two large classes: noninvasive and invasive (Figures 2A and 2B). Additional clustering of the genes further organized the data into several temporal patterns based on peak gene expression. To broadly characterize the cellular processes altered during tumor progression, we tested for enrichment of gene ontology (GO) terms in each temporal gene expression cluster. In epidermal tissue, clusters enriched for genes mediating cellular biosynthesis peaked first followed by those promoting proliferation; clusters enriched for genes involved in ECM remodeling and increased cell motility displayed maximum levels at later time points while expression of differentiation-enriched gene sets was progressively suppressed (Figure 2C). The stromal compartment displayed a markedly different pattern during tumor progression. Gene sets enriched for angiogenesis peaked rapidly, followed by a complex transcriptional reorganization of ECM-related genes and progressive induction of cell adhesion genes (Figure 2D). Interestingly, genes associated with antigen presentation were progressively repressed in the stroma, suggesting a link between tumor cell invasion and evasion of the local adaptive immune system. In total, these results suggest a model whereby tumorigenesis progresses by engaging the cellular biosynthesis machinery necessary for growth in parallel with

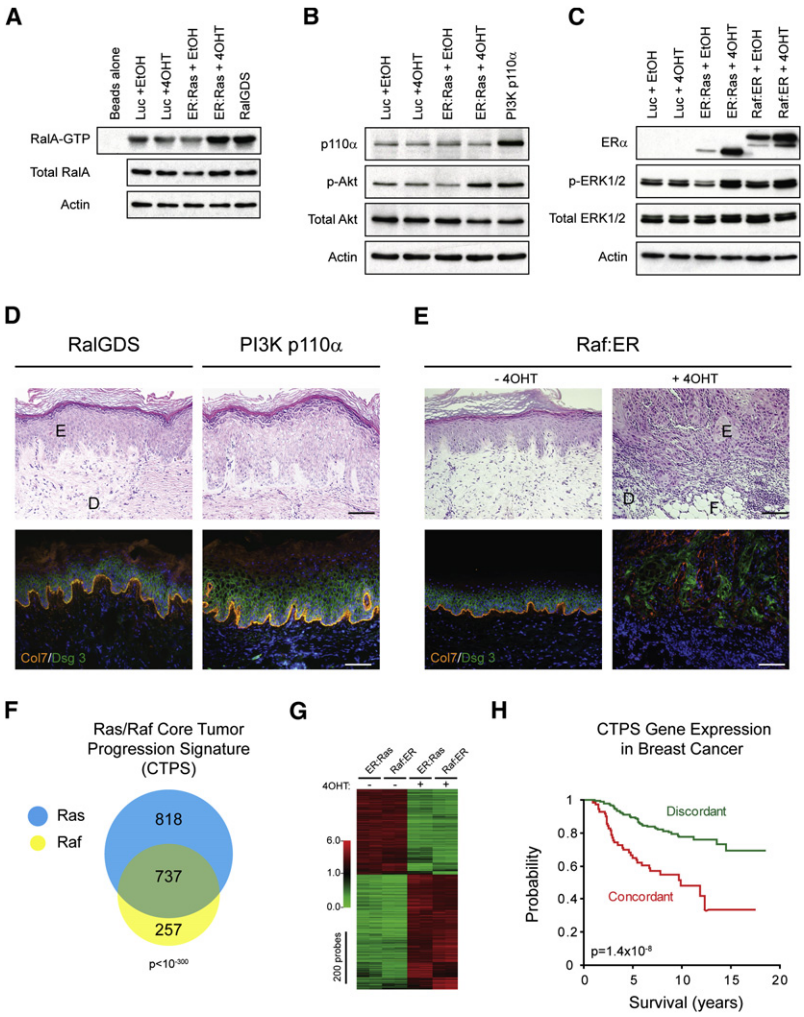


**Figure 3. Genes Coregulated during Ras- and Raf-Driven Epidermal Neoplasia Define a CTPS**

(A) Immunoblots of primary keratinocyte extracts comparing RalA-GTP levels in response to overexpression of RalGDS with 4OHT-mediated Ras activation. RalA-GTP was pulled down by incubation with a RalBD-GST fusion protein. Input cell extract (10%) was probed for total RalA and actin to verify equal loading.

(B) Immunoblots comparing levels of pAKT in response to PI3K-p110α overexpression with 4OHT-induced Ras activation. Actin serves as a loading control.

(C) Immunoblots comparing ERK phosphorylation induced by either 4OHT-mediated Raf or Ras activity. Actin serves as a loading control.

(D and E) Histology (top) of human epidermal tissue coexpressing IκBα and either active RalGDS, PI3K p110α, or Raf:ER 4 weeks after pathway activation. Note the mild hyperplasia in PI3K p110α-IκBα-expressing epidermis and invasive neoplasia in 4OHT-treated Raf:ER-IκBα transgenic tissue. E, Epidermis; D, dermis. Immunostaining (bottom) for type VII collagen (Col7; orange) and desmoglein-3 (Dsg3; green). Scale bars, 125 μm.

(F) Venn diagram illustrating the extent of transcriptional conservation between the Ras and Raf tumor signatures (p value, Fisher's exact test).

(G) Heat map representation of Ras/Raf CTPS. Note that the direction of transcriptional change is conserved between Ras and Raf signatures.

(H) Kaplan-Meier survival analysis ($p < 1.4 \times 10^{-8}$, Cox-Mantel log rank test) on 295 breast cancer samples hierarchically clustered and stratified into two classes based on similarity to the 737-gene CTPS. Patient tumors classified as concordant display a gene expression pattern analogous to that observed in the CTPS, while discordant patient tumors do not.

induction of stromal angiogenesis, followed by proliferative tumor expansion, and culminating in tumor-stromal matrix remodeling to enable tumor cell invasion.

## Genes Coregulated by Ras and Raf during Epidermal Tumorigenesis Define a Clinically Relevant Core Tumor Progression Signature

Ras interacts with and activates a myriad of downstream effector cascades to promote many of the hallmarks of cancer (Repasky et al., 2004). Activation of these downstream effectors alone or in combination can recapitulate many aspects of Ras-induced transformation (Rangarajan et al., 2004), suggesting that only a subset Ras signaling is critically required for tumorigenesis. We hypothesized that the complexity of Ras-induced gene expression could be reduced by filtering through downstream effectors sufficient to drive epidermal neoplasia. Therefore, we tested the ability of canonical effectors to replace Ras in driving human epidermal neoplasia, focusing on the Raf/MAPK, PI3K/Akt, and RalGEF/Ral signaling cascades. First, we expressed active Raf (PI3K p110α) and the RalGEF (RalGDS) in primary human keratinocytes to compare downstream pathway activation with that induced by Ras itself (Figures 3A–3C). We next examined the tumorigenic capacity of each of these Ras effectors in regenerated human epidermis. Although both the RalGDS and PI3K pathways have been implicated in human tumorigenesis in other settings, they failed to cooperate with IκBα to induce epidermal neoplasia (Figure 3D). Raf:ER-IκBα epidermis, in contrast, exhibited cardinal features of SCC, including hyperplasia, aberrant differentiation and polarity, and invasion into the underlying dermis in response to ligand-mediated Raf induction (Figure 3E). These data illustrate that, in this tissue context, Raf can mimic Ras-induced invasive epidermal neoplasia.

We next identified the genes differentially regulated between quiescent Raf:ER-IκBα epidermis and invasive, 4OHT-treated Raf:ER-IκBα tumors in order to compare this gene set to our Ras signature. This analysis resulted in 994 epithelial genes altered during Raf-driven neoplasia (Table S4). A set of 737 genes, which we term the CTPS, was shared between the Ras and Raf signatures (Figure 3F). Remarkably, the direction of CTPS gene expression was conserved for every gene between Ras and Raf (Figure 3G). Thus, Ras- and Raf-induced epidermal neoplasia share phenotypic and transcriptional similarities consistent with action via a common molecular pathway.

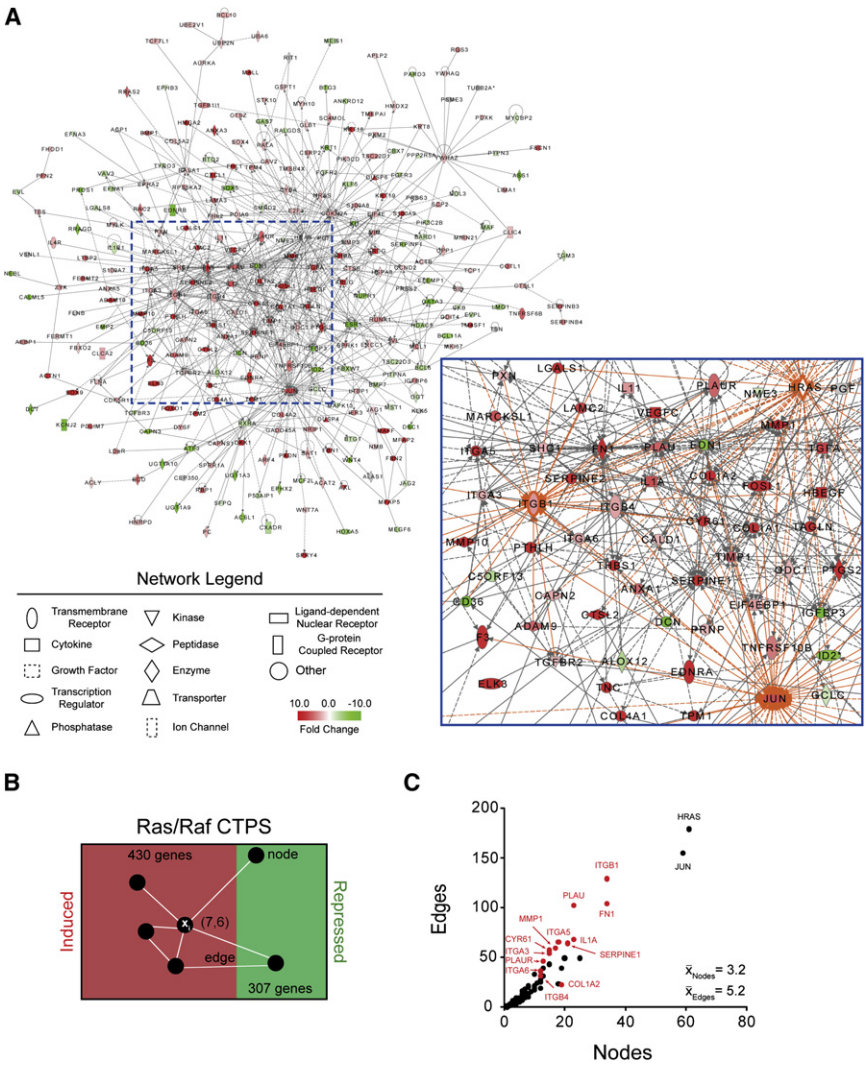


**Figure 4. CTPS Network Topology Identifies Oncogene Hubs Driving Tumorigenesis and Predicts Tumor Dependence on Matrix Interaction**

(A) A literature-based approach was used to generate a network of the physical, enzymatic, and transcriptional interactions between CTPS genes; the largest interconnected subgraph, containing 282 nodes, is shown. Nodes (genes/proteins) within the network are classified by function (shape) and colored red (induced), green (repressed), or gray (not present) based on day 35 expression values. Edges are represented as solid or dashed lines to indicate direct and indirect interactions, respectively. The dashed box is enlarged at the lower right.

(B) Schematic of the local interconnectivity ranking strategy. A network was generated for each induced CTPS member, $X_i$, linking it to any remaining members of the CTPS using the Ingenuity Knowledge Base of interactions; for each resultant network, the number of nodes and edges were plotted in (C).

(C) Interconnectivity plot of the 430 induced genes in the Ras/Raf CTPS. The average number of nodes per gene was 3.2 and the average number of edges was 5.2, with standard deviations of 5.1 and 15.3, respectively. Oncogene hubs (black) and highly interconnected extracellular nodes (red) are labeled.

To investigate the clinical relevance of the CTPS, we examined gene expression of the signature in a publicly available data set of 295 stage I and II breast cancers (van de Vijver et al., 2002). Hierarchical clustering of the tumors based on agreement with the CTPS segregated the tumors into two classes: ''concordant'' and ''discordant'' (Figure S2A). Concordant tumors had significantly poorer survival and metastasis-free survival when compared to their discordant counterparts (Figure 2H and Figure S2B, respectively). Notably, the basal-like and ERBB2+ subtypes defined by Sorlie et al. (2001) exhibit receptor tyrosine kinase activation upstream of Ras (Siziopikou and Cobleigh, 2007), correlate poorly with prognosis, and are more likely to be classified as concordant ($p < 10^{-30}$ and $p < 0.05$, respectively, Fisher's exact test). Analogous results were obtained for survival and relapse-free survival using an independent breast cancer data set (Figures S2C–S2E) (Sorlie et al., 2001). Moreover, clustering of several other epithelial tumor data sets based on CTPS gene expression consistently separated normal samples from tumor samples (Figures S2F–S2H). Pancreatic adenocarcinoma is of specific interest because this cancer is predominately Ras driven and has a <5% survival rate at 5 years. Applied to a pancreatic cancer data set (Lowe et al., 2007), the CTPS clearly differentiated pancreatic adenocarcinomas from normal pancreas and islet cell tumors (Figure S2G; $p < 10^{-12}$, Fisher's exact test). These results indicate that CTPS is a predictor of prognosis in breast cancer and is induced during tumorigenesis in a variety of epithelial cancers, including pancreatic adenocarcinoma.

## CTPS Network Topology Identifies Oncogene Hubs Driving Tumorigenesis and Predicts Tumor Dependence on Matrix Interaction

Understanding the network topology of CTPS gene and/or protein interactions may identify highly interconnected gene ''hubs'' required for tumor progression. Therefore, we utilized the Ingenuity Knowledge Base of manually curated biochemical and genetic interactions in human, mouse, and rat to construct a network interrelating the CTPS genes (Figure 4A). The CTPS network was disproportionally centered on induced genes, with Ras and the AP1 family transcription factor c-Jun standing apart as highly interconnected network hubs. The center of the network mainly comprised genes encoding ECM-interacting proteins, including proteases (*MMP1*, *MMP10*, *CAPN2*, *PLAU*, and *CTPSL2*), mediators of inflammation (*IL1A*, *IL11*, and *PTGS2*), ECM components (*COL4A1*, *COL1A1/A2*, *FN1*, *LAMC2*, *THBS1*, and *CYR61*), and integrin subunits (*ITGB1*, *ITGB4*, *ITGA3*, *ITGA5*, and *ITGA6*). Thus, global network topology implicates two oncogenes, Ras and

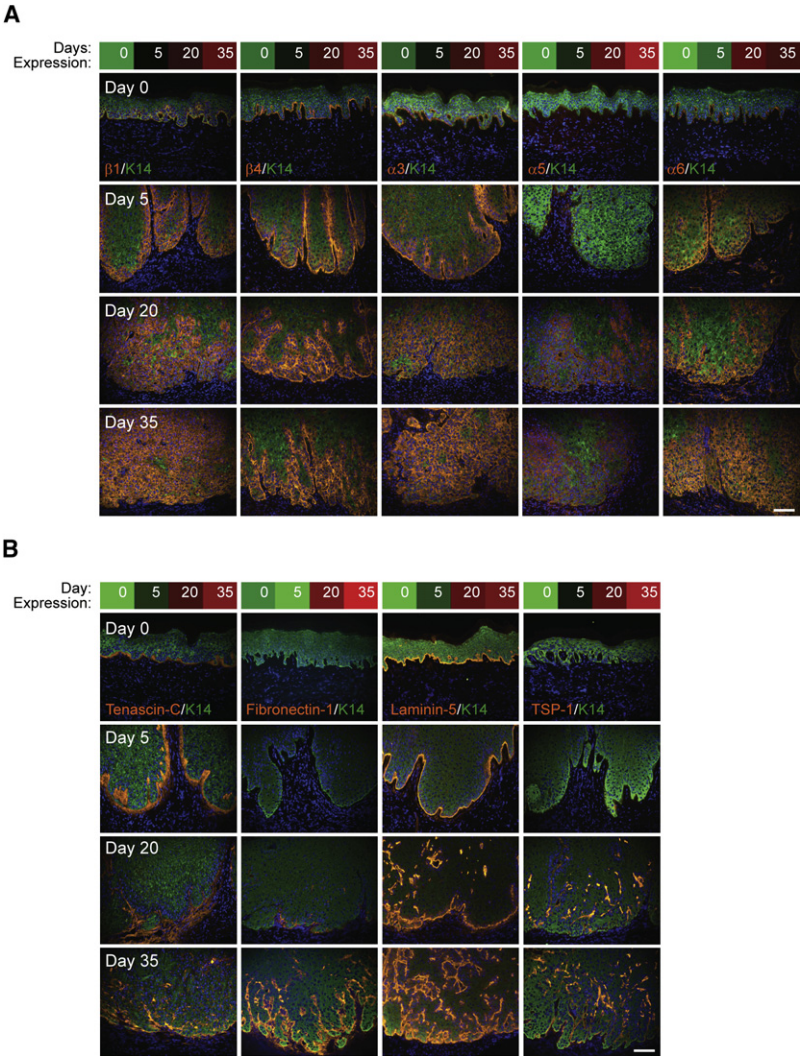


**Figure 5. Expression of Integrin Subunits and their Ligands is Temporally Induced during Neoplastic Progression**

(A) Immunostaining for differentially transcribed integrin subunits (orange) and K14 (green). Note the loss of polarity as well as the increase in the proportion of cells expressing integrin subunits during tumor progression. The corresponding time course of mRNA expression (top) for each gene is also shown. Scale bar, 125 μm.

(B) Immunostaining for the differentially expressed integrin ligands (orange) and K14 (green). TSP1 denotes thrombospondin-1. Scale bar = 125 μm.

c-Jun, as network hubs driving tumorigenesis and predicts network dependence on ECM-related molecules.

To rank the 430 upregulated CTPS genes by their local interconnectivity, we generated individual networks for each gene and plotted the corresponding number of nodes and edges (Figures 4B and 4C). As expected, Ras ranked first with 61 nodes and 179 edges, while c-Jun ranked second with 55 nodes and 155 edges. Prior work has shown that pharmacologic and genetic inhibition of c-Jun attenuates both tumor initiation and maintenance in our constitutive Ras-IκBα model (Zhang et al., 2007). To explicitly test the continual requirement of Ras activation in our inducible model, we halted 4OHT treatment to established ER:Ras-IκBα tumors. As would be predicted by both interconnectivity and prior murine tumor models using conditional Ras (Chin et al., 1999), ER:Ras-IκBα tumors reverted back to a quiescent state upon 4OHT withdrawal (Figure S3A). Thus, the two most interconnected hubs of the CTPS network, Ras and c-Jun, are required for Ras-IκBα-driven epidermal tumorigenesis.

Interaction with and modification of the tumor microenvironment is an integral component of tumor progression. Ranking CTPS members by their interconnectivity illustrates the importance of these interactions as 16 of the top 25 nodes are extracellular or cell surface proteins (Figure 4C). The β1 integrin subunit ranked third with 34 nodes and 129 edges, suggesting that its function, like that of Ras and Jun, may also be required for tumor progression. Integrins interact with the extracellular environment in both normal homeostasis and tumorigenesis (Janes and Watt, 2006). In addition to β1, several α integrin subunits known to dimerize with β1 (α3, α5, and α6), as well as several β1 integrin ligands, are also highly interconnected nodes within the CTPS network. Integrins can mediate both tumor-intrinsic and tumor-stroma interactions; therefore, we also examined β1 integrin's level of interconnectivity with genes encoding extracellular proteins differentially expressed in the stroma during tumor progression. Of the 132 extracellular members of the CTPS, the β1 integrin subunit ranked second to only Fibronectin-1, an α5β1 integrin ligand (Figures S3B and S3C). Thus, both tumor-intrinsic and tumor-stroma interconnectivity predict a functional role for the β1 integrin subunit.

To verify the gene expression data from which our network is based, we analyzed the protein expression of several ECM-related nodes within the CTPS network during Ras-driven human epidermal neoplasia. Aberrant expression of several integrin subunits has been reported in spontaneous SCC; however, staining exhibited considerable variation in these sample populations (Jones et al., 1997). Consistent with previous studies, staining for the β1, β4, α3, and α6 integrin subunits was restricted to the membrane of basal keratinocytes in quiescent epidermal tissue, while α5 subunit expression was absent. During neoplastic progression, however, integrin staining was temporally induced and expressed throughout the invasive front (Figure 5A). This temporal protein induction and spatial localization was also observed for several extracellular integrin ligands of the CTPS network (Figure 5B). Taken together, these findings confirm the gene expression data at the protein level and implicate the integrin signaling axis as a potential tumor-stromal nexus involved in Ras-driven epidermal tumor progression.

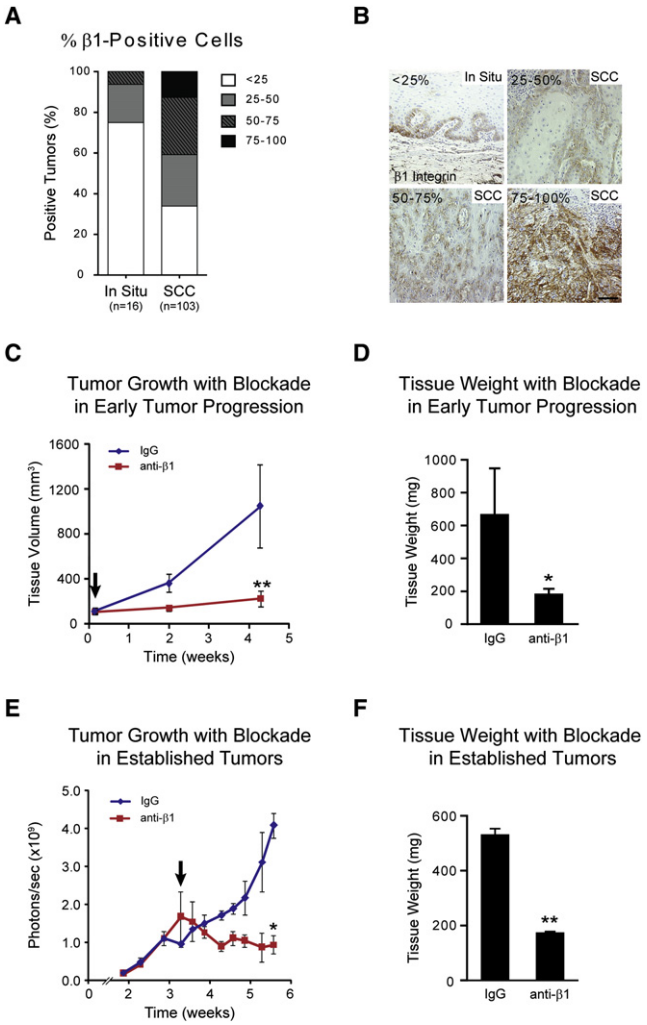


**Figure 6. The β1 Integrin Subunit Hub Is Required for Tumor Growth in Both Developing and Established Tumors**

(A) Quantitation of β1 integrin expression in SCC tissue microarrays compared to noninvasive SCC in situ patient samples. Tumors were scored based on the proportion of β1 integrin-positive epithelial cells.

(B) Representative immunostains for the data quantitated in (A). Scale bar, 125 μm.

(C) Blockade of early tumor progression. Average tumor growth in ER:Ras-IκBα grafts concomitantly treated with 4OHT and anti-β1 or IgG antibody (n = 4 mice per group, ± SD). Arrow indicates initiation of antibody treatment. **p < 0.005, Student's t test.

(D) Mean final tumor weight (± SD) from (C). *p < 0.05.

(E) Inhibition of established tumors. Average growth of Ras-IκBα-Luciferase tumors was monitored via bioluminescence following treatment with anti-β1 or IgG control antibody (n = 2 mice per group, ± SD). Arrow indicates initiation of antibody treatment. *p < 0.05.

(F) Mean final tumor weight (± SD) from (E). **p < 0.005.

## Targeting the β1 Integrin Network Hub in Developing and Established Tumors

To examine if the β1 integrin induction seen in experimental human epidermal neoplasia also occurs clinically in the progression of spontaneous SCCs, we compared β1 expression in samples from patients with preinvasive SCC in situ and invasive SCC. We scored the samples based on the percentage of epithelial cells expressing β1 integrin within the tumor mass and found that progression from benign to malignant SCC is correlated with an increase in β1 expression (Figures 6A and 6B). These data corroborate results in this model system and suggest a potential functional role for the β1 integrin subunit in human SCC progression.

To investigate a functional role for the β1 integrin subunit in our tumor model, we inhibited β1 function in developing as well as established invasive tumors using a human-specific monoclonal blocking antibody (Figure S4A) (Dittel et al., 1993). For the early tumor progression studies, ER:Ras-IκBα epidermal tissue was concomitantly treated with 4OHT and either anti-β1 or IgG control antibody for 30 days. Efficient in vivo delivery of the blocking antibody was verified by incubation of secondary antibodies against mouse IgG on tissue sections from anti-β1- and control-treated grafts (Figure S4B). Anti-β1 treatment significantly decreased tumor growth and final tissue weight when compared to IgG control treatment (Figures 6C and 6D and Figure S4C). In addition, anti-β1 treatment of established Ras-IκBα tumors halted further tumor growth in a dose-dependent manner (Figures 6E and 6F and Figures S4C–S4E). Thus, β1 integrin function is required for both early tumor progression as well as continued expansion of established tumors.

Next, we examined the histological and immunophenotypic features of anti-β1-treated tumor and control tissue to determine the mechanism by which β1 blockade inhibited Ras-driven tumorigenesis. Despite effective delivery (Figure S4B), histology of anti-β1-treated normal tissue was indistinguishable from that of IgG-treated samples (Figure 7A). In the context of 4OHT-mediated Ras activation, however, β1 inhibition resulted in epidermal tissue displaying increased differentiation and a more clearly delineated tumor-stroma border (Figures 7A and 7B). Anti-β1 treatment also significantly reduced epidermal cell proliferation compared to IgG-treated controls potentially accounting for the differences we observe in tumor size (Figure 7C). In contrast, β1 blockade did not affect the density of CD31-marked blood vessels in the stroma or the number of TUNEL-positive tumor nuclei, suggesting that angiogenesis and apoptosis both remain unaltered by antibody treatment (Figure 7D and Figures S5A and S5B, respectively). These effects were specific as knockdown of β1, but not α3 integrin, also attenuated tumor growth and enhanced tumor differentiation (Figures S6A–S6D). Thus, pharmacologic and genetic inhibition of β1 integrin function supports a tumor-intrinsic role for β1 in the promotion of Ras-driven tumor proliferation and invasion as well as the inhibition of tumor differentiation.

Our characterization of anti-β1-treated tissue suggested that β1 inhibition halted epidermal carcinogenesis prematurely in the spectrum of tumor progression. To further explore this, we profiled tumor tissue treated with anti-β1 or IgG control antibody and identified a set of 230 that genes changed ≥2-fold with anti-β1 treatment (Table S5). Clustering array samples based on these 230 genes placed the anti-β1-treated samples between days 5 and 20 in the time course of tumor progression, a position consistent with our histologic observations (Figure 7E). In contrast, IgG-treated samples clustered nearest day 35 arrays, indicating a complete progression to invasive carcinoma. GO analysis on this gene set confirmed our histologic observations, identifying the terms "extracellular region," "extracellular matrix,"

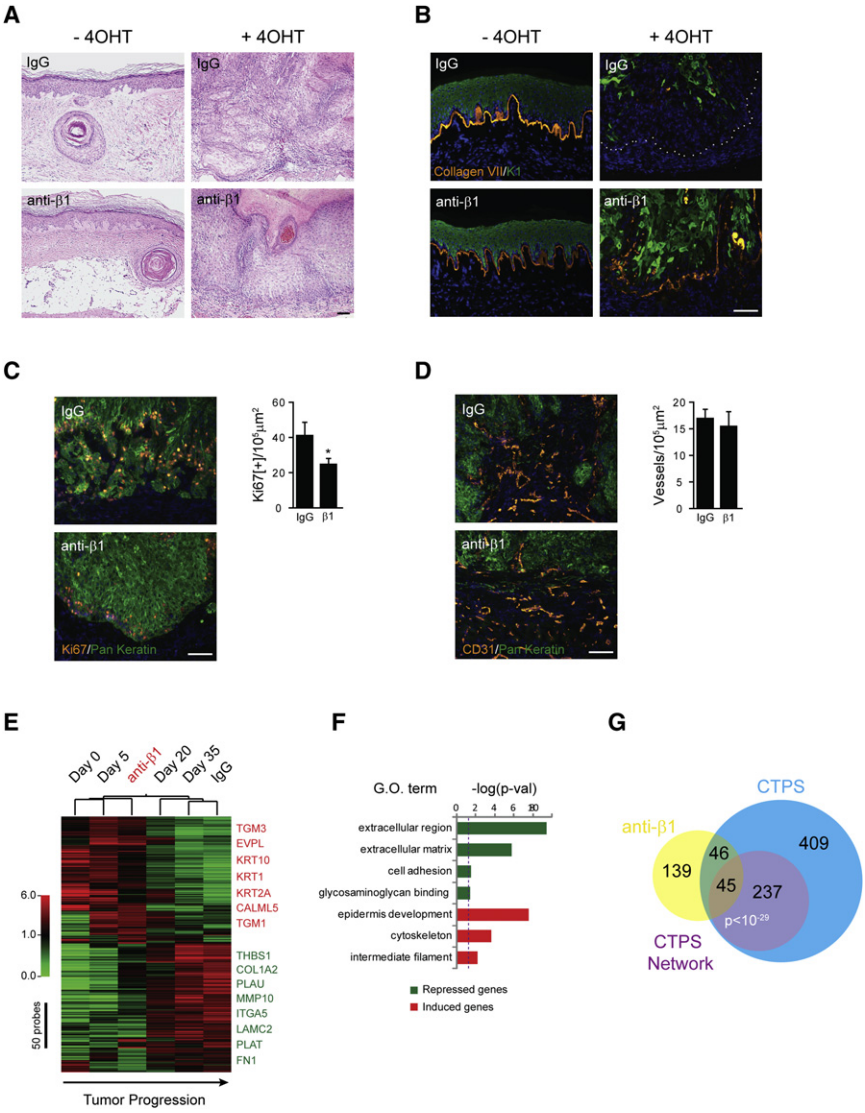


**Figure 7. β1 Integrin Blockade Disrupts CTPS Network Gene Expression, Decreases Tumor Proliferation, and Restores Tumor Differentiation**

(A) Histology of ER:Ras-IκBα grafts ± 4OHT and treated with either anti-β1 or IgG antibody for 30 days. Note the reduced hyperplasia, increased polarity, and decreased tumor-stroma intermixing with anti-β1 treatment. Scale bar, 125 μm.

(B) Expression of the differentiation marker keratin 1 (K1; green) and type VII collagen (Col7; orange). Note that anti-β1 treatment partially preserves differentiation and BM protein distribution. Scale bar, 125 μm.

(C) Immunostaining for the proliferation marker Ki67 (orange) and pan-keratin (green). Scale bar, 125 μm. Graph depicts the mean number (± SD) of Ki67-positive epithelial cells after the indicated treatment (n = 4 grafts per group). *p < 0.05, Student's t test.

(D) Immunostaining for the endothelial marker CD31 (orange) and pan-keratin (green). Scale bar, 125 μm. Graph depicts the mean vessel density (± SD) after the indicated treatment (n = 4 grafts per group).

(E) Heat map of the 230 genes altered ≥2-fold by anti-β1-mediated blockade of early tumor progression. LCM was used to isolated tumor RNA from ER:Ras-IκBα grafts cotreated with 4OHT and either anti-β1 or IgG antibody for 30 days. Duplicate array samples were averaged and hierarchically clustered; the dendogram at the top represents the extent of similarity among samples. Selected induced (red) and repressed (green) genes are indicated. Note that anti-β1-treated tumors cluster in between days 5 and 20.

(F) Significantly enriched GO terms for genes induced (red) and repressed (green) by β1 blockade are represented in a histogram as the −log ($p < 0.05$, Bonferroni-corrected EASE score). Redundant terms have been omitted for clarity. Dotted line represents the significance threshold.

(G) Venn diagrams depicting the overlap between the genes altered with anti-β1 treatment, the Ras/Raf CTPS, and the CTPS network. Significance was calculated using a Fisher's exact test.

and "cell adhesion" as enriched in genes suppressed by β1 blockade, while the terms "epidermis development" and "intermediate filament" were enriched in genes induced by anti-β1 treatment (Figure 7F and Figures S7A and S7B). We also observed a significant overlap between genes present in the CTPS network and those altered by anti-β1 treatment ($p < 10^{-29}$, Fisher's exact test). If tumor dependence is truly correlated with network interconnectivity, CTPS network members should be preferentially affected by β1 inhibition when compared to their non-network counterparts. Indeed, we find a significant enrichment of CTPS network genes in the 91 CTPS genes affected by β1 blockade (Figure 7G; $p < 0.05$, Fisher's exact test). Moreover, all CTPS network genes affected by β1 inhibition shifted their expression toward that of the quiescent profile, whereas 8 of the remaining 46 overlapping CTPS genes still exhibited the tumor profile (Figure S7C). Taken together, these data confirm that β1 blockade arrests tumor development prematurely, illustrate that hub targeting disproportionally disrupts network gene expression, and suggest that the CTPS network faithfully models the genetic and biochemical interactions necessary for epidermal neoplastic progression.

## DISCUSSION

Here, we generated an inducible model of human tissue neoplasia recapitulating cardinal features of human SCC development, which allowed temporal characterization of gene expression in both epithelium and stroma during tumor progression. This differed from other studies analyzing spontaneous human tumor precursors and cancers (Gius et al., 2007; Haider et al., 2006) by not only eliminating variability in genetic background and heterogeneity due to genomic instability but also

by avoiding dilution by the many precursor lesions that never progress to invasive cancer. Among Ras effectors, Raf proved capable of driving progression to invasive neoplasia. Filtering the Ras profile by Raf-induced gene expression distilled a CTPS that correlated with clinical malignancy of several types of human epithelial cancer. Network modeling of the genetic and biochemical interactions between CTPS genes/proteins was used to prioritize functional targets. Genes encoding ECM-related proteins potentially involved in tumor-stroma crosstalk showed a high degree of interconnectivity in the CTPS network and functional blockade of one such highly interconnected ECM network hub, the β1 integrin subunit, attenuated experimental tumor progression in vivo. Thus, integrating inducible human tissue neoplasia, temporal gene expression profiling, and network modeling provides a tractable platform to predict and validate potential targets in a human tissue context.

Carcinogenesis involves sequential changes in the epithelial tumor cells, as well as in multiple nontransformed cell types and the ECM of the surrounding stromal microenvironment. Using LCM to characterize the transcriptional profiles of adjacent tumor and stroma during neoplastic progression, a sequence of gene expression changes associated with strikingly different biologic processes was discerned in each tissue compartment. During early tumor progression, the epithelial transcriptome was characterized by induction of cellular biosynthesis and tumor proliferation. Likewise, early stromal gene expression promoted tumor expansion via induction of transcripts involved in angiogenesis. Neoplastic invasion requires that malignant cells migrate, survive, and proliferate outside their intended microenvironment. Correspondingly, genes regulating ECM remodeling, cell motility, and cell adhesion peaked during invasive stages of tumorigenesis. In addition, the onset of invasion was marked by a decrease in transcription of cell cycle genes. It is possible that physical limitations in nutrient diffusion begin to impede further growth as stromal transcription of angiogenic factors plateaus prior to invasion. However, specific isolation and subsequent gene expression profiling of rat adenocarcinoma cells actively migrating has also demonstrated a reduction in the expression of cell cycle genes during invasion (Wang et al., 2004). Thus, it is likely that invasive behavior of tumor cells occurs at the expense of maximal cellular proliferation.

Modification of the local immune environment represents an important aspect of tumor progression. Proinflammatory signals are known to positively influence carcinogenesis by facilitating ECM remodeling, angiogenesis, and lymphogenesis (Coussens and Werb, 2002). Accordingly, we observed an upregulation of several potent mediators of inflammation, including *TGFA*, *PTGS2*, *IL1A*, and *IL1B*. In contrast, a significant number of genes encoding proteins involved in antigen presentation were repressed in the stromal compartment. Despite severely impaired lymphocyte function, antigen presentation cells function normally in severe combined immunodeficient mice (Czitrom et al., 1985). This pattern of gene expression suggests that local adaptive immune surveillance would generally inhibit epidermal tumor progression. Indeed, reduced expression of genes mediating adaptive immunity distinguish papillomas with a high incidence of conversion to SCC from low risk counterparts (Darwiche et al., 2007). Moreover, renal transplant patients undergoing chronic immune suppression exhibit 250-fold greater incidence of SCCs (Hartevelt et al., 1990). Taken together, our tumor and stromal gene expression profiles present a dynamic picture of the biologic processes unfolding during tumor progression and provide a framework to guide future investigations into the interactions between tumor cells and their stromal microenvironment (Figure S8).

Substantial evidence suggests that oncogenic Ras signaling proceeds through different downstream effector pathways dependent on the species and cell type examined (Repasky et al., 2004). We find that the Raf/MAPK cascade is capable of driving human epidermal neoplasia and profiling of these tumors illustrates that only a portion of the transcriptional output of Ras is required for tumorigenesis. More broadly, the Ras/Raf CTPS shows that the increased signaling specificity of downstream molecules can be used as effective biologic filters of gene expression in lieu of arbitrarily increasing the stringency of statistical parameters. The CTPS is largely distinct from previously identified Ras signatures, sharing 10 genes with a K-Ras signature derived from a murine lung adenocarcinoma model (Sweet-Cordero et al., 2005) and 68 genes with a signature derived from H-Ras overexpression in cultured human mammary epithelial cells (Bild et al., 2006). These discrepancies are likely due to different bioinformatic and experimental approaches, but may also reflect species and cell type specificities in Ras signaling. For instance, oncogenic K-Ras is competent to drive murine lung carcinogenesis, whereas constitutively active B-Raf generally produces only benign neoplasia (Dankort et al., 2007). However, the correlation we observe between CTPS gene expression and that seen in multiple human epithelial cancers known to involve Ras pathway activation suggests that significant similarities in Ras signaling exist across multiple human epithelial tissues in vivo, irrespective of the effectors responsible for mediating Ras's effects.

Prioritizing CTPS network genes by tumor and stromal interconnectivity identified the β1 integrin subunit, which is overexpressed in many malignancies, as an important mediator of human epidermal tumor progression. β1 integrin activity is known to modulate keratinocyte differentiation in culture (Evans et al., 2003) and ectopic expression of specific β1 integrin receptors enhances chemical-induced transformation of murine epidermis (Janes and Watt, 2006). Here, we show that both pharmacologic and genetic inhibition of β1 function attenuate human epidermal neoplastic progression by repressing proliferation and restoring differentiation. The species specificity of the blocking antibody used precludes analysis of the systemic effects of anti-β1 treatment, a potential concern given the lethality observed with deleting *Itgb1* during embryogenesis in a variety of tissues, including skin (Raghavan et al., 2000). However, postnatal deletion of *Itgb1* in murine epidermis produces only mild interfollicular abnormalities (Lopez-Rovira et al., 2005) and we observe no effect of β1 blockade on quiescent epidermis. Consistent with our findings, somatic deletion of murine *Itgb1* in mammary epithelium reduces tumor proliferation, but has no effect on normal mammary ductal outgrowth (White et al., 2004). Moreover, antibody-mediated repression of β1 has no effect on nontransformed mammary epithelial cell lines in three-dimensional cell culture, but induces apoptosis and reduces proliferation of several breast cancer cell lines both in culture and in vivo (Park et al., 2006). Utilizing our inducible model, we further illustrate that anti-β1 treatment is effective against both

developing and established invasive tumors, which is an important consideration for an efficacious cancer treatment. Taken together, these findings indicate a tumor-intrinsic requirement for β1 function during tumorigenesis and suggest that β1 blockade may represent an attractive oncotherapeutic for a variety of human epithelial tumors.

Our approach complements tumor sequencing efforts (Wood et al., 2007) and alternative networking strategies (Pujana et al., 2007) aimed at identifying cancer-associated genes, but differs from many profiling approaches by the potential to identify specific targets outside of driving oncogenes (Bild et al., 2006). Although inhibition of β1 preferentially affected the gene expression of CTPS network members, validating our method, several non-network members were also altered, indicating that the network is incomplete. Additional proteomic and genomic data sets could be incorporated to generate a more comprehensive CTPS network as well as to reduce the potential bias toward well-studied genes inherent to any literature-based networking strategy. Interrogating other highly interconnected nodes within the CTPS network will likely identify more potential targets, begin to establish topologic criteria correlated with consistent functional consequences, and enhance understanding of the mechanisms of human cancer progression.

## EXPERIMENTAL PROCEDURES

### Retroviral Constructs and Cell Culture

The LZRS-based retroviral constructs for IκBαM (IκBα), ER$^{TM}$:H-Ras$^{G12V}$ (ER:Ras), ΔRaf$_{DD}$-1:ER$^{TM}$ (Raf:ER), PI3K p110α:CAAX (PI3K), and RalGDS:CAAX (RalGDS) have been described previously (Dajee et al., 2003, 2002; Harada et al., 2005; Tarutani et al., 2003). Virus production and keratinocyte culture were performed as previously described (Choate et al., 1996). Briefly, transfection of the phoenix 293T packaging cell line to produce viral supernatant was achieved using Fugene 6.0 (Roche) according to the manufacturer's protocol. Primary human keratinocytes were isolated from neonatal foreskin specimens and cultured at 37°C with 5% $CO_2$ in a 1:1 mixture of undefined keratinocyte SFM (GIBCO) and keratinocyte medium 154 (Cascade Biologics). For infection, 15% confluent 10 cm plates of keratinocytes were incubated with 12 ml of 0.45 μm filtered viral supernatant containing polybrene (5 μg/ml) and subjected to low-speed centrifugation (300 × g) for 1 hr at 32°C. Serial infections separated by 10–14 hr intervals were utilized to introduce multiple genes.

### Animal Studies

Engineered keratinocytes were seeded onto devitalized human dermis and grafted onto female CB.17 *scid/scid* mice as previously described (Choate et al., 1996; Dajee et al., 2003). ER:Ras-IκBα grafts were allowed to heal for 4–16 weeks. Ras activation was achieved via daily intraperitoneal injections of 4OHT (730 μg) dissolved in a mixture of corn oil and ethanol (Reuter and Khavari, 2006). Time course data is representative of two independent experiments; human tissue was excised and analyzed every 5 days (n = 2 grafts/time point). For Ras effector experiments, PI3K-IκBα- or RalGDS-IκBα-expressing skin (n = 4 grafts/group) was harvested 4 weeks after grafting, while Raf:ER-IκBα (n = 4 grafts) was excised after 4 weeks of 4OHT treatment. Early tumor progression studies were done on ER:Ras-IκBα grafted animals (n = 4/group) concomitantly treated with 4OHT and subcutaneous injection (0.5 mg in sterile PBS; three times/week) of a monoclonal blocking antibody (P5D2) against β1 integrin (Dittel et al., 1993) or mouse IgG control; grafts were analyzed after 30 days of treatment. Uninduced ER:Ras-IκBα control grafts (n = 2/group) were also treated with either P5D2 or mouse IgG and harvested at 30 days. Anti-β1 or IgG treatment of established tumors (n = 2/group) was done on Ras-IκBα-Luciferase-expressing grafts and began 3 weeks after grafting. Tumor growth was quantitated by measuring volume or total bioluminescent flux (photons/sec) using an IVIS-100 imaging system and LivingImage 3.0 software (Xenogen). Statistical significance of β1 blockade on tumor growth and final weight was determined using an unpaired two-tailed Student's t test. All experiments involving human tissue or animals were approved by the Stanford University Human Subjects Institutional Review Board and Animal Care and Use Committee, respectively.

### Laser Capture Microdissection and Microarrays

For laser capture microdissection (LCM), 7 μm cryosections were stained with cresyl violet according to the manufacturer's protocol (LCM staining kit; Ambion). A Leica AS LMD system was used to isolate epithelial cells from biologic duplicates of the following samples: day 0, 5, 20, and 35 ER:Ras-IκBα grafts; day 30 Raf:ER-IκBα grafts ± 4OHT; and day 30 ER:Ras-IκBα grafts ± 4OHT and treated with either P5D2 or mouse IgG. Adjacent stromal tissue was isolated in parallel duplicates. Total RNA (100–200 ng) was purified, subjected to one round of T7-based linear amplification, and fragmented according to the manufacturer's protocol (RNAqueous-Micro, MessageAmp II-Biotin Enhanced; Ambion). Labeling and hybridization of RNA to either human (HG-U133A 2.0) or mouse (MG-430A 2.0) Affymetrix GeneChips was performed by the Stanford Protein and Nucleic Acid Facility.

### Protein Expression Analysis

For all antibody catalog numbers and conditions, see Table S6. Western blot analysis for pERK1/2 and pAkt was performed on lysates from infected primary keratinocytes cultured in supplement-free media containing 4OHT (50 nM in ethanol) or vehicle for 24 hr. RalA-GTP pull downs were performed as described (Tarutani et al., 2003) using 50 μg of total protein extract from cells treated as above. For tissue microarrays, nonoverlapping skin SCC arrays (SK801 and SK802; US Biomax) and a panel of SCC in situ patient samples were deparaffinized, rehydrated, and digested with protease XXV (1 mg/ml; Thermo Scientific) for 5 min at 37°C. Sections were then incubated with a mouse anti-β1 antibody (Abcam) followed by Vectastain R.T.U. ABC Elite Reagent (Vector Labs). Peroxidase activity was detected using 3,3′-diaminobenzidine (Dako).

### Data Analysis

For all microarray experiments, arrays were robust multichip average normalized; probes were mean centered, clustered, and visualized with GeneSpring GX 7.3 software using a red-green color scale. Unless otherwise noted, differential expression required passing the following filters: multiclass Significance Analysis of Microarrays 3.0 with a false discovery rate less than 5% (Tusher et al., 2001), an average fold change greater than or equal to two at any time point, and an average raw expression intensity ≥100 at any time point. For future analyses, signatures were converted from Affymetrix probe IDs to unique Entrez Gene IDs. Five genes (Entrez IDs: 3184, 3490, 5228, 5317, and 8992) in the Ras signature and one gene in the Raf signature (10492) were removed because they had two separate probes whose expression values went both up and down. p values indicating the significance of the overlap between various signatures were calculated using a Fisher's exact test. GO term enrichment was performed using DAVID with the total set of genes on the appropriate microarray as the background; p values represent a Bonferroni-corrected modified Fisher's exact test (Huang et al., 2009). Similar findings were obtained independently with the KEGG database. The CTPS network was constructed using the Ingenuity Knowledge Base to connect members of the CTPS; default settings were used, except that the molecules were limited to CTPS members (IPA 6.0; Ingenuity Systems, Inc.). Similarly, the connectivity plots were generated by constructing individual networks between each of the 430 upregulated CTPS genes and the remainder of the CTPS, followed by manual counting of the edges and nodes. Kaplan-Meier survival analysis of the Netherlands Cancer Institute data set of 295 breast cancers was done, as previously described (Chang et al., 2005), using a Cox-Mantel log rank test performed by WinStat software (R Fitch Software).

## ACCESSION NUMBERS

Microarray data described herein are publicly available in the NCBI Gene Expression Omnibus under accession number GSE15299.

## SUPPLEMENTAL DATA

Supplemental Data contain Supplemental Experimental Procedures, eight figures, and six tables and can be found with this article online at http://www.cell.com/cancer-cell/supplemental/S1535-6108(09)00116-0.

## ACKNOWLEDGMENTS

We thank D.W. Felsher, J. Sage, A. Sweet-Cordero, M.P. Scott, J. Ford, D. Fisher, S.E. Artandi, A.E. Oro, M.P. Marinkovich, P.A. Dumesic, T.W. Ridky, G.L. Sen, A.B. Truong, D.E. Webster, and Z. Siprashvili for helpful discussions and for critical analysis of this work; D.I. Barragan for technical assistance; N.T. Nguyen for assistance purifying the P5D2 antibody; E. Zhou for microarray hybridization and scanning; and J.L. Rinn and D.J. Wong for bioinformatic guidance. This work was supported by the U.S. Veterans Affairs Office of Research and Development and by National Institutes of Health/National Institute of Arthritis and Musculoskeletal and Skin Diseases grants AR43799 and AR49737 to P.A.K.

Received: October 2, 2008
Revised: January 22, 2009
Accepted: April 6, 2009
Published: June 1, 2009

## REFERENCES

Alam, M., and Ratner, D. (2001). Cutaneous squamous-cell carcinoma. N. Engl. J. Med. *344*, 975–983.

Albert, R., Jeong, H., and Barabasi, A.L. (2000). Error and attack tolerance of complex networks. Nature *406*, 378–382.

Bild, A.H., Yao, G., Chang, J.T., Wang, Q., Potti, A., Chasse, D., Joshi, M.B., Harpole, D., Lancaster, J.M., Berchuck, A., et al. (2006). Oncogenic pathway signatures in human cancers as a guide to targeted therapies. Nature *439*, 353–357.

Chang, H.Y., Nuyten, D.S., Sneddon, J.B., Hastie, T., Tibshirani, R., Sorlie, T., Dai, H., He, Y.D., van't Veer, L.J., Bartelink, H., et al. (2005). Robustness, scalability, and integration of a wound-response gene expression signature in predicting breast cancer survival. Proc. Natl. Acad. Sci. USA *102*, 3738–3743.

Chin, L., Tam, A., Pomerantz, J., Wong, M., Holash, J., Bardeesy, N., Shen, Q., O'Hagan, R., Pantginis, J., Zhou, H., et al. (1999). Essential role for oncogenic Ras in tumour maintenance. Nature *400*, 468–472.

Choate, K.A., Kinsella, T.M., Williams, M.L., Nolan, G.P., and Khavari, P.A. (1996). Transglutaminase 1 delivery to lamellar ichthyosis keratinocytes. Hum. Gene Ther. *7*, 2247–2253.

Coussens, L.M., and Werb, Z. (2002). Inflammation and cancer. Nature *420*, 860–867.

Czitrom, A.A., Edwards, S., Phillips, R.A., Bosma, M.J., Marrack, P., and Kappler, J.W. (1985). The function of antigen-presenting cells in mice with severe combined immunodeficiency. J. Immunol. *134*, 2276–2280.

Dajee, M., Tarutani, M., Deng, H., Cai, T., and Khavari, P.A. (2002). Epidermal Ras blockade demonstrates spatially localized Ras promotion of proliferation and inhibition of differentiation. Oncogene *21*, 1527–1538.

Dajee, M., Lazarov, M., Zhang, J.Y., Cai, T., Green, C.L., Russell, A.J., Marinkovich, M.P., Tao, S., Lin, Q., Kubo, Y., et al. (2003). NF-kappaB blockade and oncogenic Ras trigger invasive human epidermal neoplasia. Nature *421*, 639–643.

Dankort, D., Filenova, E., Collado, M., Serrano, M., Jones, K., and McMahon, M. (2007). A new mouse model to explore the initiation, progression, and therapy of BRAFV600E-induced lung tumors. Genes Dev. *21*, 379–384.

Darwiche, N., Ryscavage, A., Perez-Lorenzo, R., Wright, L., Bae, D.S., Hennings, H., Yuspa, S.H., and Glick, A.B. (2007). Expression profile of skin papillomas with high cancer risk displays a unique genetic signature that clusters with squamous cell carcinomas and predicts risk for malignant conversion. Oncogene *26*, 6885–6895.

Dittel, B.N., McCarthy, J.B., Wayner, E.A., and LeBien, T.W. (1993). Regulation of human B-cell precursor adhesion to bone marrow stromal cells by cytokines that exert opposing effects on the expression of vascular cell adhesion molecule-1 (VCAM-1). Blood *81*, 2272–2282.

Evans, R.D., Perkins, V.C., Henry, A., Stephens, P.E., Robinson, M.K., and Watt, F.M. (2003). A tumor-associated beta 1 integrin mutation that abrogates epithelial differentiation control. J. Cell Biol. *160*, 589–596.

Ganter, B., and Giroux, C.N. (2008). Emerging applications of network and pathway analysis in drug discovery and development. Curr. Opin. Drug Discov. Devel. *11*, 86–94.

Gius, D., Funk, M.C., Chuang, E.Y., Feng, S., Huettner, P.C., Nguyen, L., Bradbury, C.M., Mishra, M., Gao, S., Buttin, B.M., et al. (2007). Profiling microdissected epithelium and stroma to model genomic signatures for cervical carcinogenesis accommodating for covariates. Cancer Res. *67*, 7113–7123.

Haider, A.S., Peters, S.B., Kaporis, H., Cardinale, I., Fei, J., Ott, J., Blumenberg, M., Bowcock, A.M., Krueger, J.G., and Carucci, J.A. (2006). Genomic analysis defines a cancer-specific gene expression signature for human squamous cell carcinoma and distinguishes malignant hyperproliferation from benign hyperplasia. J. Invest. Dermatol. *126*, 869–881.

Harada, K., Truong, A.B., Cai, T., and Khavari, P.A. (2005). The class II phosphoinositide 3-kinase C2beta is not essential for epidermal differentiation. Mol. Cell. Biol. *25*, 11122–11130.

Hartevelt, M.M., Bavinck, J.N., Kootte, A.M., Vermeer, B.J., and Vandenbroucke, J.P. (1990). Incidence of skin cancer after renal transplantation in The Netherlands. Transplantation *49*, 506–509.

Huang, D.W., Sherman, B.T., and Lempicki, R.A. (2009). Systematic and integrative analysis of large gene lists using DAVID bioinformatics resources. Nat. Protoc. *4*, 44–57.

Janes, S.M., and Watt, F.M. (2006). New roles for integrins in squamous-cell carcinoma. Nat. Rev. Cancer *6*, 175–183.

Jeong, H., Mason, S.P., Barabasi, A.L., and Oltvai, Z.N. (2001). Lethality and centrality in protein networks. Nature *411*, 41–42.

Jones, J., Watt, F.M., and Speight, P.M. (1997). Changes in the expression of alphav integrins in oral squamous cell carcinomas. J. Oral Pathol. Med. *26*, 63–68.

Jonsson, P.F., and Bates, P.A. (2006). Global topological features of cancer proteins in the human interactome. Bioinformatics *22*, 2291–2297.

Khavari, P.A. (2006). Modelling cancer in human skin tissue. Nat. Rev. Cancer *6*, 270–280.

Lee, I., Lehner, B., Crombie, C., Wong, W., Fraser, A.G., and Marcotte, E.M. (2008). A single gene network accurately predicts phenotypic effects of gene perturbation in *Caenorhabditis elegans*. Nat. Genet. *40*, 181–188.

Lewis, K.G., and Weinstock, M.A. (2007). Trends in nonmelanoma skin cancer mortality rates in the United States, 1969 through 2000. J. Invest. Dermatol. *127*, 2323–2327.

Littlepage, L.E., Egeblad, M., and Werb, Z. (2005). Coevolution of cancer and stromal cellular responses. Cancer Cell *7*, 499–500.

Lopez-Rovira, T., Silva-Vargas, V., and Watt, F.M. (2005). Different consequences of beta1 integrin deletion in neonatal and adult mouse epidermis reveal a context-dependent role of integrins in regulating proliferation, differentiation, and intercellular communication. J. Invest. Dermatol. *125*, 1215–1227.

Lowe, A.W., Olsen, M., Hao, Y., Lee, S.P., Taek Lee, K., Chen, X., van de Rijn, M., and Brown, P.O. (2007). Gene expression patterns in pancreatic tumors, cells and tissues. PLoS ONE *2*, e323.

Mueller, M.M., and Fusenig, N.E. (2004). Friends or foes - bipolar effects of the tumour stroma in cancer. Nat. Rev. Cancer *4*, 839–849.

Orimo, A., Gupta, P.B., Sgroi, D.C., Arenzana-Seisdedos, F., Delaunay, T., Naeem, R., Carey, V.J., Richardson, A.L., and Weinberg, R.A. (2005). Stromal fibroblasts present in invasive human breast carcinomas promote tumor growth and angiogenesis through elevated SDF-1/CXCL12 secretion. Cell *121*, 335–348.

Park, C.C., Zhang, H., Pallavicini, M., Gray, J.W., Baehner, F., Park, C.J., and Bissell, M.J. (2006). Beta1 integrin inhibitory antibody induces apoptosis of

breast cancer cells, inhibits growth, and distinguishes malignant from normal phenotype in three dimensional cultures and in vivo. Cancer Res. *66*, 1526–1535.

Pujana, M.A., Han, J.D., Starita, L.M., Stevens, K.N., Tewari, M., Ahn, J.S., Rennert, G., Moreno, V., Kirchhoff, T., Gold, B., et al. (2007). Network modeling links breast cancer susceptibility and centrosome dysfunction. Nat. Genet. *39*, 1338–1349.

Raghavan, S., Bauer, C., Mundschau, G., Li, Q., and Fuchs, E. (2000). Conditional ablation of beta1 integrin in skin. Severe defects in epidermal proliferation, basement membrane formation, and hair follicle invagination. J. Cell Biol. *150*, 1149–1160.

Rangarajan, A., Hong, S.J., Gifford, A., and Weinberg, R.A. (2004). Species- and cell type-specific requirements for cellular transformation. Cancer Cell *6*, 171–183.

Repasky, G.A., Chenette, E.J., and Der, C.J. (2004). Renewing the conspiracy theory debate: does Raf function alone to mediate Ras oncogenesis? Trends Cell Biol. *14*, 639–647.

Reuter, J.A., and Khavari, P.A. (2006). Use of conditionally active ras fusion proteins to study epidermal growth, differentiation, and neoplasia. Methods Enzymol. *407*, 691–702.

Siziopikou, K.P., and Cobleigh, M. (2007). The basal subtype of breast carcinomas may represent the group of breast tumors that could benefit from EGFR-targeted therapies. Breast *16*, 104–107.

Sorlie, T., Perou, C.M., Tibshirani, R., Aas, T., Geisler, S., Johnsen, H., Hastie, T., Eisen, M.B., van de Rijn, M., Jeffrey, S.S., et al. (2001). Gene expression patterns of breast carcinomas distinguish tumor subclasses with clinical implications. Proc. Natl. Acad. Sci. USA *98*, 10869–10874.

Sweet-Cordero, A., Mukherjee, S., Subramanian, A., You, H., Roix, J.J., Ladd-Acosta, C., Mesirov, J., Golub, T.R., and Jacks, T. (2005). An oncogenic KRAS2 expression signature identified by cross-species gene-expression analysis. Nat. Genet. *37*, 48–55.

Tarutani, M., Cai, T., Dajee, M., and Khavari, P.A. (2003). Inducible activation of ras and raf in adult epidermis. Cancer Res. *63*, 319–323.

Tusher, V.G., Tibshirani, R., and Chu, G. (2001). Significance analysis of microarrays applied to the ionizing radiation response. Proc. Natl. Acad. Sci. USA *98*, 5116–5121.

van de Vijver, M.J., He, Y.D., van't Veer, L.J., Dai, H., Hart, A.A., Voskuil, D.W., Schreiber, G.J., Peterse, J.L., Roberts, C., Marton, M.J., et al. (2002). A gene-expression signature as a predictor of survival in breast cancer. N. Engl. J. Med. *347*, 1999–2009.

Wang, W., Goswami, S., Lapidus, K., Wells, A.L., Wyckoff, J.B., Sahai, E., Singer, R.H., Segall, J.E., and Condeelis, J.S. (2004). Identification and testing of a gene expression signature of invasive carcinoma cells within primary mammary tumors. Cancer Res. *64*, 8585–8594.

White, D.E., Kurpios, N.A., Zuo, D., Hassell, J.A., Blaess, S., Mueller, U., and Muller, W.J. (2004). Targeted disruption of beta1-integrin in a transgenic mouse model of human breast cancer reveals an essential role in mammary tumor induction. Cancer Cell *6*, 159–170.

Wong, D.J., Liu, H., Ridky, T.W., Cassarino, D., Segal, E., and Chang, H.Y. (2008). Module map of stem cell genes guides creation of epithelial cancer stem cells. Cell Stem Cell *2*, 333–344.

Wood, L.D., Parsons, D.W., Jones, S., Lin, J., Sjoblom, T., Leary, R.J., Shen, D., Boca, S.M., Barber, T., Ptak, J., et al. (2007). The genomic landscapes of human breast and colorectal cancers. Science *318*, 1108–1113.

Yildirim, M.A., Goh, K.I., Cusick, M.E., Barabasi, A.L., and Vidal, M. (2007). Drug-target network. Nat. Biotechnol. *25*, 1119–1126.

Zhang, J.Y., Adams, A.E., Ridky, T.W., Tao, S., and Khavari, P.A. (2007). Tumor necrosis factor receptor 1/c-Jun-NH2-kinase signaling promotes human neoplasia. Cancer Res. *67*, 3827–3834.